

Localization at interfaces of imperfect AlSb/InAs heterostructures

M. J. Shaw

Department of Physics, The University of Newcastle upon Tyne, Newcastle upon Tyne, United Kingdom

(Received 2 March 1998)

The properties of a variety of imperfect AlSb/InAs heterostructures have been studied, using *ab initio* pseudopotential calculations to include a microscopic description of the interfaces themselves. Substitutional group IV defects were investigated at a number of lattice sites, acting as both donor and acceptor impurities. The interaction between silicon donor defects and the interfaces is shown to result in the formation of localized resonances that alter the optical and transport characteristics of the structures. The detailed form of the localized features is found to be sensitive to structural disorder close to the interfaces.

[S0163-1829(98)07835-7]

I. INTRODUCTION

The microscopic features of heterointerfaces, and their role in determining the optical and transport characteristics of semiconductor microstructures, is emerging as one of the key issues in semiconductor physics.¹⁻⁷ As advances in growth techniques enable the realization of abrupt interfaces with nearly perfect atomic arrangement, the discrepancy between experimental data and the predictions of conventional theoretical descriptions of quantum confined electron and hole wave functions is becoming apparent. In particular, the origin of room-temperature luminescence observed in SiGe quantum well structures cannot be accounted for by conventional theory.⁸⁻¹⁰ Most of the theoretical work on semiconductor heterostructures available in the literature is based upon the semiclassical picture of the interface, as an abrupt step in the potential moving from one material into the next, described in terms of the valence-band-offset parameter.¹¹ While such methods have proven to be successful in predicting many of the essential physical properties of electron and hole states confined by quantum wells, they fail to account for features in the observed optical spectra. Clearly the physical mechanism driving the luminescence is absent from the existing theoretical account of heterostructures. Even with the inclusion of interface disorder and reconstruction,^{12,13} features to which the anomalous spectral features are commonly attributed, models founded upon semiclassical steplike interfaces remain at odds with experiment. Could the microscopic variations of the potential in the region of the interface bonds themselves provide the key to understanding the optical spectra?

In recent papers this question has been addressed for the case of SiGe.¹² Turton and Jaros¹ examined a number of possible mechanisms for the luminescence and outlined the arguments that implicate interface localization as the origin of the luminescence. In order to investigate the precise role that the interfaces play it is necessary to go beyond the semiclassical interface model. In other words, it is necessary to consider a model in which the full microscopic fluctuations in the potential throughout the interface region is included. Such a model may be achieved by applying the local density approximation of density functional theory with *ab initio* pseudopotentials. While such methods have been applied

many times to the study of heterostructures,¹⁴⁻¹⁶ and even directly to studies of interface properties, the physical features that have been focused upon are those associated with the confinement of charge on the scale of the quantum wells themselves (e.g., offsets, miniband energies, etc.). In a recent study, we applied these *ab initio* techniques to the case of SiGe superlattice structures with a variety of substitutional defects situated adjacent to the interfaces.² Analysis of the localized defect resonances in these structures indicates that the microscopic interaction between the defects and the interface itself results, in the case of antimony defects, in a strong coupling, modifying the nature of the charge localization and providing a possible mechanism for the breakdown of selection rules derived using conventional theory. These results indicate that the microscopic properties of the interface itself, the “intra-facial” properties, could provide the mechanism for the luminescence features observed in SiGe quantum wells, and opens up a new framework within which to understand the optical spectra and transport properties of heterostructures.

A class of materials that is currently generating considerable interest, particularly in the field of infrared optoelectronics, is AlSb/GaSb/InAs.¹⁷⁻²² By careful choice of layer dimensions and alloy compositions heterostructure systems developed from these materials are able to offer a number of favorable features. Deep conduction wells may be engineered in conjunction with extremely high mobilities to enhance the characteristics for a number of device applications.²³ The degree of freedom arising from the three compatible semiconductors and their alloys enables a wide variety of heterostructures to be conceived, with fundamental gaps spanning a wide range of frequencies. One particular family of structures that has already been the subject of considerable theoretical and experimental effort is AlSb/InAs superlattices.^{24,25} In addition to the technological importance associated with these structures, their microscopic interface structure has already attracted a great deal of attention. The absence of a common anion between the two layers leads to the possibility of two chemically different interface formations. Depending on the precise shutter sequencing during MBE growth the interfaces can be formed between In and Sb ions, InSb-like, or Al and As ions, AlAs-like.²⁶ It has been shown by experiment that the physical properties of AlSb/

InAs superlattices can be altered by specifying the interface configurations in this way.²⁵ Recently, we presented a series of *ab initio* pseudopotential calculations demonstrating the differentiation of interface type, and supporting the hypothesis that localized interface-related states are formed at perfect InSb-like interfaces.³

Most theoretical studies of interfaces in AlSb/InAs structures have, so far, concentrated on the properties of defect-free interfaces, or on weak isovalent substitutional defects at the interfaces. Primarily, the questions that have been asked relate to the origin of the background carrier concentrations present in such structures.^{27–30} While such a debate has illuminated many interesting features associated with the interface formation, the interface localizations identified belong to a different class from those that arise in the SiGe structures, and with which we are concerned in the present paper. In the case of localization at the essentially perfect InSb-like interfaces, the formation of the localized states may be qualitatively understood by invoking a particle-in-a-box picture of the interface, in which the InSb interface bonds are regarded as an ultranarrow InSb quantum well. Full-scale microscopic calculations are required principally to confirm that the essential features are correctly described by such a picture, and provide justification for the interpretation so given. This class of localized states has been discussed in some detail by us elsewhere in the literature.^{2,31,32} By contrast, the localized features that arise as a result of the defect-interface interaction, studied here for the case of heterovalent defects in AlSb/InAs superlattices, cannot be predicted using a semiclassical interface model. Rather, these features are a result of the microscopic properties of the interface itself, providing a whole facet of heterostructure behavior unavailable to semiclassical models.

In this paper we use *ab initio* pseudopotential calculations to examine a series of interfacial imperfections in AlSb/InAs superlattices, and in particular to identify the interface-induced localizations that occur. The imperfections that we consider include a variety of group IV substitutional defects at a number of different lattice sites, and in addition we consider the cases of some two-atom lattice imperfections. However, our study focuses primarily on the case of a substitutional Si donor impurity in the InAs layer adjacent to the interface. The localized resonance that we observe for this defect is in close analogy with the Sb donor resonances observed in SiGe systems, and is indicative of a strong defect-interface coupling. This evidence suggests that the microscopic “intraface” region plays an important role in determining the behavior of AlSb/InAs superlattices, and that a full microscopic description of the interfaces is essential to our understanding of the physical properties of these heterostructures.

II. THEORETICAL METHOD

The theoretical model that we have used to describe the imperfect superlattice structures is that of the local density approximation (LDA) of density functional theory with *ab initio* pseudopotentials. Density functional theory and the LDA have been discussed in great depth in the literature, and we shall not reproduce the details here.³³ For the purposes of the current study this method presents many advantages over

alternative, and simpler, techniques such as empirical pseudopotential or effective-mass theory. Since we are concentrating primarily on the physical effects associated with the microscopic features of the interfaces, and the nature of their interaction with isolated defects, our choice of model is governed by its ability to describe the potential in the interface region. While empirical techniques are well suited to describing features of quantum well systems that occur on the scale of the quantum well width, and where the deviation from bulk is relatively small, they are not able to describe so well features such as the microscopic interface potential. Indeed, the empirical-pseudopotential technique, often used for studies of superlattice systems usually invokes an abrupt step in the potential at the interface, clearly failing to take into account the microscopic potential variations in this region. In contrast, the self-consistent charge density determined by the LDA approach has no such step enforced upon it. The use of transferable atomic pseudopotentials, derived with reference to the free atom states, enables these key microscopic features at which the bulklike character of the potentials is broken, to be fully described. Specifically, the *ab initio* pseudopotentials of Bachelet *et al.*³⁴ are used.

The calculations presented in this paper adopt the formalism of Jones³⁵ and Briddon,³⁶ initially developed for the study of large clusters of atoms and here extended to work within a periodic or supercell geometry. In this, the wave function is expanded in a set of Gaussian basis functions. These functions are multiplied by spherical harmonics to impart the *s*- and *p*-like character of the atomic orbitals. To provide a sufficiently accurate description of the charge density sixteen of these basis functions were centered on each atom. We apply this method to systems of periodically repeated unit cells containing up to 128 atoms. During the calculations the positions of all of the atoms were relaxed individually in order to minimize the total energy of the self-consistent ground state of each structure studied.

While the study of isolated substitutional defects in superlattices demands unit cells large in all three dimensions, the computational demands of the *ab initio* approach restrict the sizes of the unit cells that can practically be tackled. In order to enable unit cells with reasonable dimensions in the plane of the interfaces we restrict our study to short period superlattices, namely, 2AlSb/2InAs (where 2AlSb refers to 2 lattice constants AlSb). This period provides us with what remain well-confined valence and conduction states while allowing eight primitive superlattice unit cells to be included in the plane of the interfaces. A schematic representation of the unit cell studied is shown in Fig. 1. The dimensions of the supercell in the plane of the interfaces are determined by the lattice constant of the nominal substrate, chosen to be AlSb, as determined by *ab initio* calculations. The overall length of the supercell in the growth direction is determined by minimization of the calculated total energy for the perfect 2AlSb/2InAs structure. Of course, such a unit cell is clearly not sufficiently large to provide a description of truly isolated defects, and in particular does not allow the Coulombic shallow donor state to be properly accounted for. However, we are not concerned at present with the extended features of the defect states, such as the shallow donor and excitonic levels. Rather, our attention is focused upon the short-range effects

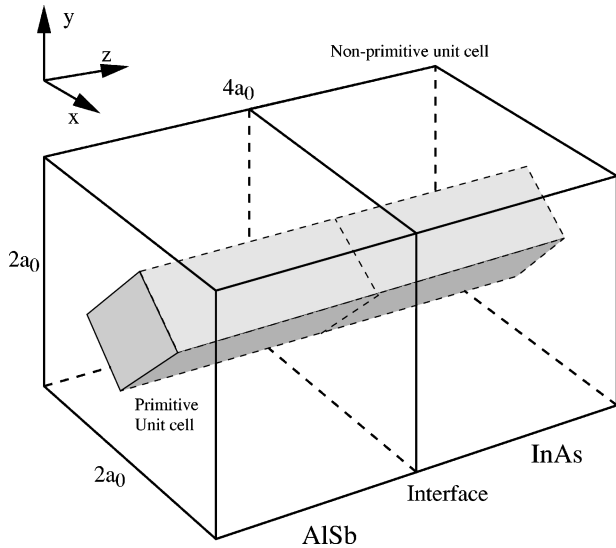


FIG. 1. Schematic diagram of the nonprimitive unit cell containing eight atomic spirals of the perfect $2\text{AlSb}/2\text{InAs}$ superlattice. Also shown is the relation to the primitive unit cell of the same structure.

arising through the interaction of the defect with the intrafacial potential profile.

In order to assist in the interpretation of the results that are obtained from the full-scale calculations, it is useful to develop a simple intuitive model of the defect. The defect molecule model, illustrated schematically in Fig. 2 provides just such a picture.³⁷ First we consider the band structure of a perfect bulk semiconductor from which a single atom is removed. The vacancy so created leaves four unbonded sp^3 orbitals, which symmetrize to form a series of levels in the gap, one of A_1 symmetry and a T_2 triplet. We then consider bringing in a defect atom with free-atom s and p orbitals to fill the vacancy. The states of the same symmetry interact to form bonding and antibonding combinations indicated in Fig. 2. The model predicts A_1 bonding and antibonding resonances, A_1B and A_1A close to the bottom of the valence and conduction bands, respectively, and T_2 bonding and anti-

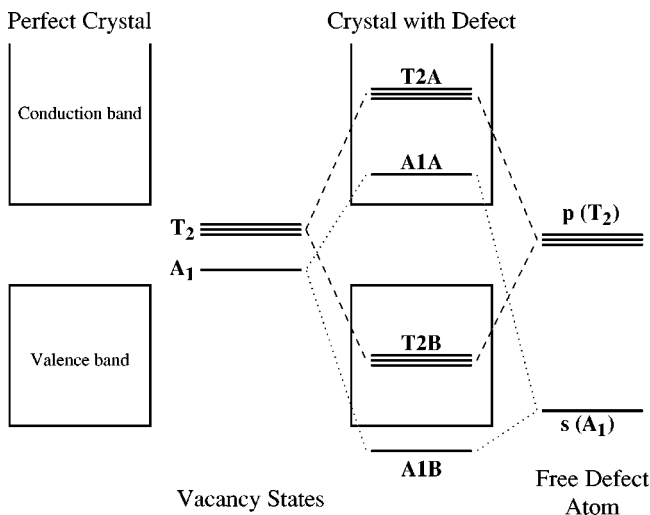


FIG. 2. Schematic diagram representing the simple defect molecule model for a defect in a bulk crystal.

bonding resonances T_2B and T_2A deep inside the valence and conduction bands, respectively. These are the defect resonances that one expects to obtain from the full scale calculation. Of course, it must be remembered that this is only an extremely simple qualitative model, and no account is taken of the microscopic interaction with the lattice. The defect molecule model does not allow us to make any predictions concerning the energies of the resonances, but merely provides a useful framework within which to discuss the results of our microscopic calculations. Note also that the model is described above for the case of a bulk material—while the basic features of this may be directly transferred to the case of a microstructure, the symmetry labels applied to the resonances should be altered to refer to the lower point group of the system. However, in the interests of clarity it is advantageous to retain the labeling appropriate to the bulk case, without loss of meaning in the context of the present study. It must be stressed once again that the defect molecule model is invoked only to help us to interpret the *ab initio* results, and is not used for any calculations.

III. THE PERFECT $2\text{AlSb}/2\text{InAs}$ SUPERLATTICE

Before the effect of substitutional defects can be addressed it is necessary to obtain a full understanding of the states in the perfect superlattice system. For studies of the perfect superlattice it is, of course, not necessary to use the 128-atom unit cell shown in Fig. 1. Where the translational symmetry in the plane of the interfaces is unbroken by defects the primitive unit cell contains a single atomic spiral of just 16 atoms. However, since our goal is ultimately to provide comparison with the imperfect structures, for which the larger cell is required, it is useful to perform calculations using the nonprimitive unit cell for the perfect structure. This provides insight into the effects of zone folding, and allows us to identify the origin of the states at the zone center.

For the perfect superlattice it is instructive to compare the Brillouin zones corresponding to the primitive and 128-atom non-primitive unit cells. The relationship between these is illustrated in Fig. 3. The smaller reciprocal lattice vectors associated with the non-primitive unit cell result in a small Brillouin zone (SBZ) eight times smaller than that of the primitive cell. As a result, each wave vector in the SBZ is equivalent to seven additional vectors in the full Brillouin zone, which translate to it through reciprocal lattice vectors of the nonprimitive cell. A calculation performed at the wave vector in the SBZ will generate the states associated with all eight wave vectors in the primitive unit cell. This is the so-called zone-folding mechanism. The eight wave vectors that “fold” onto the zone center (Γ) of the SBZ are indicated in Fig. 3 (where the points lie on the Brillouin zone boundaries only one of the equivalent wave vectors is shown). It is clear from Fig. 3, then, that the states at Γ for the 128-atom unit cell will include states originating at Γ in the primitive cell in addition to states folded from wave vectors (100) , $(\pm\frac{1}{2}, \frac{1}{2}, 0)$, $(\pm\frac{1}{2}, 0, 0)$, and $(0, \pm\frac{1}{2}, 0)$ (all wave vectors in units of $2\pi/a$, where a is the substrate lattice constant).

Figure 4 shows the superlattice band structure calculated along some of the symmetry lines for the primitive unit cell. The band structure calculated for the nonprimitive unit cell is superimposed. Comparison of the two band structures for

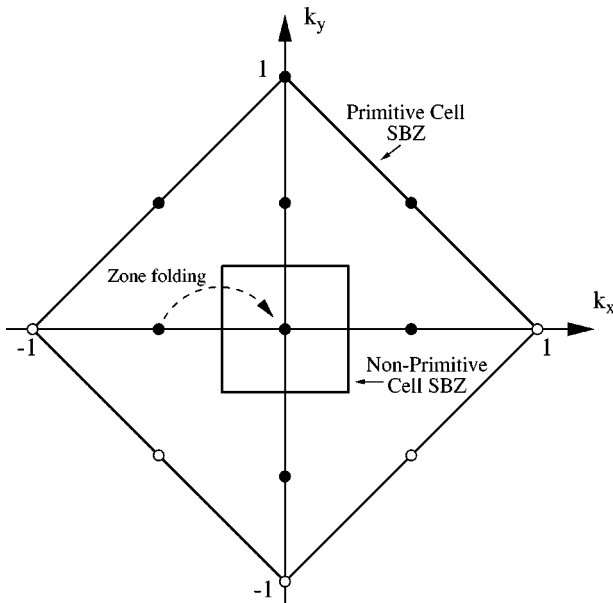


FIG. 3. The relation between the superlattice small Brillouin zone (SBZ) of the primitive and nonprimitive units cells of Fig. 1, shown schematically in the plane parallel to the interfaces. The solid circles represent the points which “fold” onto the zone center of the SBZ of the nonprimitive cell. The open circles lying on the edge of the primitive SBZ are wave vectors that are translated by a reciprocal lattice vector of the primitive cell from, and hence equivalent to, other “folding” wave vectors.

what is physically an identical system enables the origin of the energy levels in the nonprimitive cell to be identified. Some of the key states at the zone center of the nonprimitive system have been labeled according to the wave vector in the primitive-cell zone at which they originate. The bulk origin of these states can then be identified by comparison with the band structures of the bulk constituents, invoking a zone-

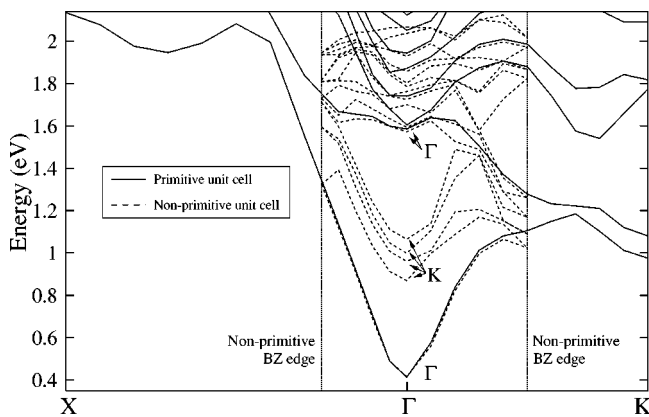


FIG. 4. The calculated band structure of the 2AlSb/2InAs superlattice is plotted for the primitive unit cell along the symmetry lines Γ -X and Γ -K where Γ is the zone center where K is the point lying at the boundary of the superlattice Brillouin zone on the [110] axis. The band structure obtained for the calculation of the same structure using the nonprimitive unit cell is superimposed over the smaller volume of wave vector space corresponding to its unit cell. Some of the key folded states at the zone center have been labeled according to the wave vector in the primitive Brillouin zone from which they originate.

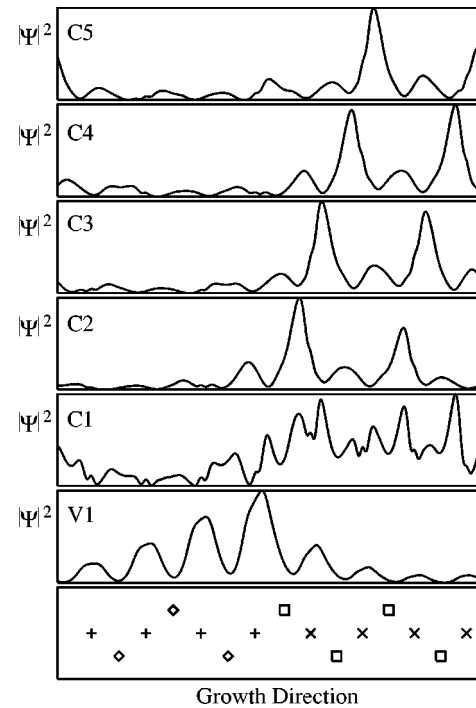


FIG. 5. The charge density (arbitrary units) of some of the zone-center states in the nonprimitive 2AlSb/2InAs calculation, integrated over the plane parallel to the interface, is plotted against position along the growth axis. The charge density is shown for the valence-band edge state, V1, the lowest Γ derived conduction state, C1, and the conduction states C2-C5 folded from the $(2\pi/a)(\pm\frac{1}{2}, \frac{1}{2}, 0)$ wave vectors. The positions of the atomic planes are indicated at the bottom where \diamond represents Al, + represents Sb, \square represents In, and \times represents As.

folding argument applied to the reduction in Brillouin zone on moving from bulk to superlattice unit cell. Of course, in this case, the zone-folding mechanism is slightly different since the bulk unit cell does not represent the full system. As a result of the perturbation arising from the different layers the superlattice energies are not exactly the energies of the folded bulk wave vectors, though it is often possible to deduce the bulk origin from the energies. The ground state of the nonprimitive superlattice calculation is found to be derived from the InAs Γ conduction minimum. However, the four states occurring at 0.85–1.05 eV are derived from the folded L valley of the bulk InAs (the bulk states being folded onto the $(\pm\frac{1}{2}, \frac{1}{2}, 0)$ wave vector of the primitive superlattice Brillouin zone). The first excited Γ states do not occur until energies of ≈ 2.2 eV. The bulk origin of these states is important when one comes to predict the optical properties of the structures.

The charge densities of the highest valence state and lowest five conduction states at Γ in the perfect 2AlSb/2InAs superlattice, integrated over the plane parallel to the interfaces, are plotted along the growth axis in Fig. 5. The valence band-edge state is clearly localized towards the InSb-like interface. We previously observed such an effect in longer period AlSb/InAs superlattices,³ and it reflects the microscopic potential arising from the InSb bonds across the interface. As discussed earlier in this paper, such localization is clearly distinct from the interface-related localization at defects, which is the subject of the present paper. The asym-

metric interface configuration, one AlAs-like and one InSb-like, is reflected also in the form of the conduction-band charge densities. In addition, the nature of the charge density of the conduction states of bulk L -valley origin is clearly distinct from the zone-center derived conduction ground state.

The states of the perfect superlattice that have been described in this section provide a background for the defect resonances in which we are primarily interested.

IV. DONOR DEFECT RESONANCES

A. Substitutional Si

The defect that we shall study in considerable detail is the substitutional Si defect, where the Si takes the place of an In atom in the lattice (denoted Si_{In}). On such a site the Si atom acts as a donor in the InAs layers, and indeed Si is commonly introduced intentionally to the growth procedure in order to n -dope InAs layers. The behavior of Si_{In} defects is therefore of practical interest to device performance. For the short-period superlattices described in the previous section there are four inequivalent sites for such a defect. The total energy was calculated for the optimized structure for each of these defect sites in order to determine the most likely position of the defect. In each case the 128-atom unit cell of Fig. 1 was used. These calculations indicate that the most energetically favorable position for the defect is that of the In atom bonded to the Sb across the InSb-like interface, approximately 0.2 eV lower than the alternative sites. We shall therefore restrict our attention to this particular Si_{In} defect.

Before we analyze in detail the nature of the electronic states in this structure, it is important that we assess the stability of relaxed atomic positions we predict. The total energy calculations described above used as initial positions the relaxed positions of the perfect superlattice. Starting from this highly symmetrical initial configuration, the relaxation predicted by our calculations was essentially constrained to a simple relaxation of bond lengths in which the initial symmetry is retained (unless rounding errors were to permit a symmetry breaking relaxation). To test whether a lower energy configuration might exist in which the overall symmetry is reduced the calculations were repeated with the initial atom positions randomly perturbed, and with the defect atom moved off the lattice site. For each of the calculations, the atoms converged to the symmetrical positions predicted by the initial calculation, indicating that the interface defect structure first predicted is indeed relatively stable. However, it must be recognized that the limited size of the unit cell prevents the formation of any large scale reconstructions about the defect atom, so the absolute stability of the defect structure predicted cannot be assured.

For the Si_{In} donor impurity the defect molecule model (Fig. 2) predicts an antibonding (A_{1A}) resonance of s symmetry, lying close to the conduction-band edge. It was the A_{1A} resonance that demonstrated such interesting interface-related effects in the case of Sb donors in SiGe superlattices.² We therefore examine in detail the electronic structure close to the bottom of the conduction band. Localized A_{1A} resonances are identified lying ≈ 1.3 eV above the band edge. The wave functions associated with these resonances contain a mixture of unperturbed (perfect) wave functions spanning a

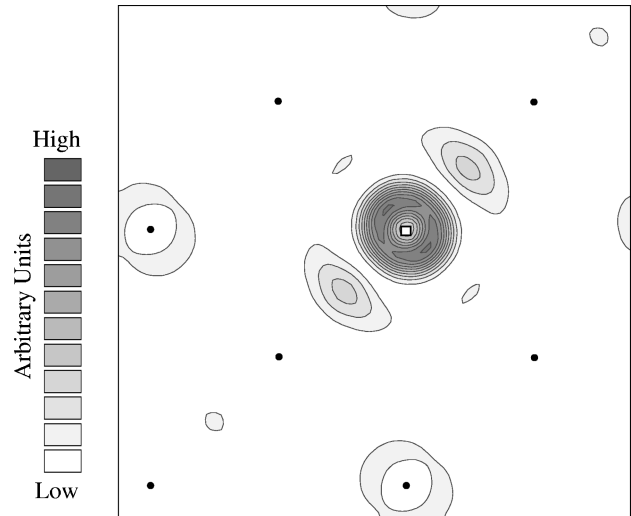


FIG. 6. The charge density (arbitrary units) associated with the A_{1A} resonance of the Si_{In} defect in the 2AlSb/2InAs superlattice, plotted in the plane parallel to the interfaces, passing through the defect atom. The projection of the positions of the In atoms that were located in this plane prior to relaxation are indicated by solid circles, while the open box indicates the position of the Si atom.

wide range of energies. Figure 6 shows the charge density of the principal resonance level, plotted in the plane parallel to the interfaces passing through the defect atom. The A_1 symmetry of the resonance is clearly reflected in the charge density distributions. Note that there is a considerable dispersion of the A_{1A} resonance due to the relatively small unit cell studied, reflected in significant charge localization for a number of energy levels.

To isolate the effect of the interfaces in determining the form of the defect resonances, it is necessary to compare with the resonance of the Si_{In} defect in bulk InAs. The difference between the behavior of the donor defect in bulk and superlattice reflects the strength of the defect-interface coupling. Calculations were repeated for the same Si_{In} defect in bulk InAs, strained to an AlSb substrate to directly compare with the InAs layers in the strained superlattice. The charge density of the key A_{1A} resonance level is plotted in Fig. 7, in the plane parallel to the substrate surface and passing through the defect. It can clearly be seen that the axial form that the resonance adopts in the presence of the interfaces (Fig. 6) is absent in the bulk situation. Rather, the defect in the bulk induces a near-spherical resonance. The introduction of the interface is therefore seen to significantly modify the form of the defect resonance.

At this point it is useful to make a comparison with the case of Sb donors in SiGe superlattices (studied in detail by Shaw *et al.*²). The A_{1A} resonance of the Sb_{Si} defect occurred at the very edge of the conduction band. It was found that the form of the localized charge density was altered with respect to the same defect in bulk Si, reflecting a strong coupling with the microscopic interface potential. A clear axial shape is apparent in the charge density of the Sb_{Si} resonance, which is compared to the Si_{In} case in Fig. 8. While the extent of the axial form is greater in the case of the Sb_{Si} , the general form of the two resonances is similar. This suggests that as in the SiGe systems, the microscopic interface poten-

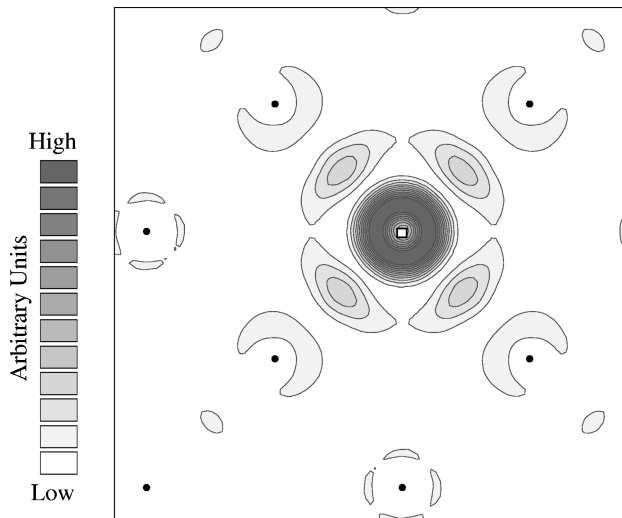


FIG. 7. The charge density (arbitrary units) associated with the $A1A$ resonance of the Si_{In} defect in bulk InAs, plotted in the plane parallel to the surface, passing through the defect atom. The projection of the positions of the In atoms that were located in this plane prior to relaxation is indicated by solid circles, while the open box indicates the position of the Si atom.

tial in the AlSb/InAs superlattices modifies the localized features of substitutional donor defects.

B. Substitutional C

So far, we have demonstrated the effect of the interaction between the superlattice interfaces and an Si defect in AlSb/InAs structures. Does this effect occur with all substitutional donors, or is it dependent on the specific properties of the Si atom? To test whether the coupling is present simply by virtue of there being a donor, or whether the process is sensitive to the chemical nature of the particular defect, we performed a calculation for substitutional C_{In} defects. Although

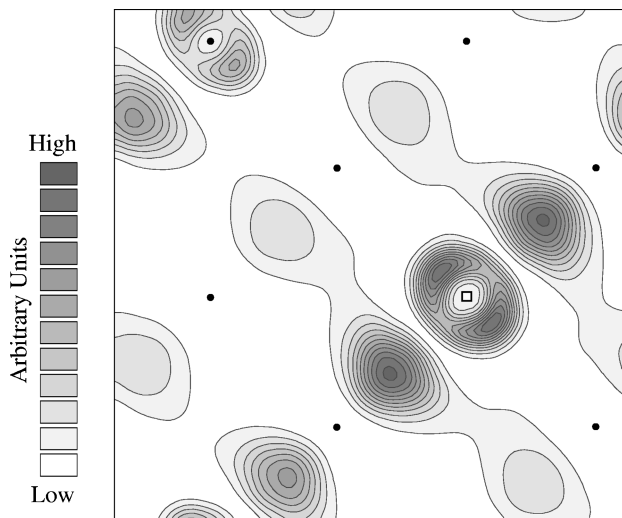


FIG. 8. The charge density (arbitrary units) associated with the $A1A$ resonance of the Sb_{Si} defect in the 1Si/1Ge superlattice, plotted in the plane parallel to the interfaces, passing through the defect atom. The projection of the positions of the Si atoms that were located in this plane prior to relaxation are indicated by solid circles, while the open box indicates the position of the Sb atom.

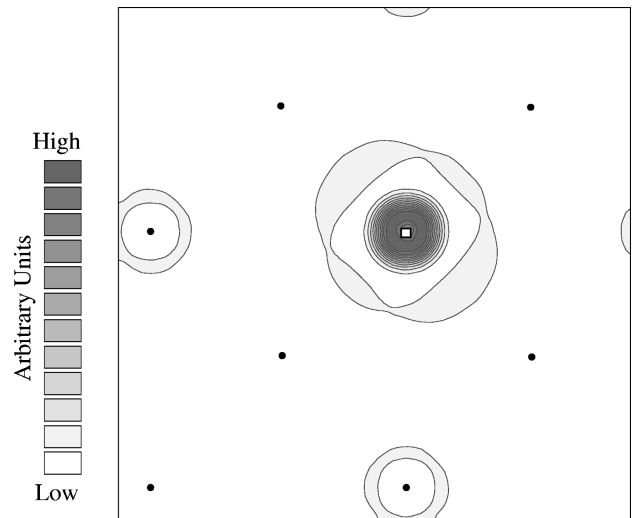


FIG. 9. The charge density (arbitrary units) associated with the $A1A$ resonance of the C_{In} defect in the 2AlSb/2InAs superlattice, plotted in the plane parallel to the interfaces, passing through the defect atom. The projection of the positions of the In atoms that were located in this plane prior to relaxation are indicated by solid circles, while the open box indicates the position of the C atom.

such defects do not in fact represent particularly likely defects in real systems, and are consequently not of great interest *per se*, their chemical similarity to the Si as group IV donors allows for a useful comparison.

The introduction of a C_{In} defect modifies the electronic structure of the superlattice in broadly the same manner as the Si defect. A principal $A1A$ resonance can be identified, located some way above the conduction-band edge, with a wave function whose characteristics correspond to a combination of the perfect system wave function over a large energy subspace. In addition, there is once again considerable dispersion associated with the $A1A$ resonance, with significant localization of charge across a range of energies. However, there are significant differences in the detail of the C_{In} resonance structure. Firstly, the calculations predict a deeper resonance for the C defect the $A1A$ resonance is formed lower in the band than the corresponding level in Si structure. This is in keeping with the fact that the C atom is considerably smaller and induces a far larger distortion to the lattice. However, perhaps most significantly, the coupling to the interfaces, reflected in the axial perturbation to the $A1A$ resonance of Si_{In} , is radically different in the case of C_{In} . The charge density associated with the C_{In} resonance is plotted parallel to the interface plane in Fig. 9. Comparison with Figs. 6 and 7 shows that the resonance of the C_{In} defect in the *superlattice* closely resembles that of the Si_{In} in *bulk*, as opposed to that of Si_{In} in the superlattice. The C_{In} resonance is largely unaffected by the presence of the interfaces. Clearly, then, the interaction between the defect and interface is sensitive to the microscopic properties of the defect itself. In other words, the chemical properties of the defect atom itself are critical in determining the nature of its coupling to the interfaces. Specifically, the calculations indicate that the interaction with the interfaces is considerably stronger for the silicon donor than for the carbon.

Further, it is interesting to note that the larger defect-interface effects that occur for silicon occur in spite of the

fact that the lattice relaxation induced is considerably smaller than for the carbon defect. Indeed, the change in the nearest-neighbor bond length is more than four times as large for the carbon defect as for the silicon. It is apparent, then, that not only does the chemical nature of the defect affect the interface-related localization, but that in fact it is dominant over the effect of lattice relaxation. A parallel may again be drawn to the situation in SiGe superlattices, where a similar distinction has been demonstrated between the behavior of substitutional Sb and As defects. Detailed studies of defect resonances in SiGe have shown conclusively that the discrepancy arises principally as a result of the chemical nature of the defect rather than through the difference in the degree of lattice relaxation.³⁸ To identify the precise chemical properties that govern the interface interaction, that is, to identify exactly what is special about Si_{In} (as opposed, for example, to C_{In}), would require a detailed study encompassing a number of other defects, and lies beyond the scope of the present study. However, from the calculations presented so far it can be concluded that the interesting interface-related localization observed for Si_{In} defects is a consequence of the particular microscopic properties of Si atoms in conjunction with the intrafacial potential.

V. ACCEPTOR IMPURITY RESONANCES

Let us now turn our attention to the case of Si defects acting as acceptor impurities in the AlSb layers, Si_{Sb} . Specifically, we shall consider the substitution of one of the Sb ions in the plane forming the InSb-like interfaces. We wish to compare and contrast with the behavior of the donor Si_{In} impurities discussed in the previous section. Once again, the *ab initio* pseudopotential calculations are used to determine the relaxation of the lattice, to examine its stability, and to compute a self-consistent charge density for the system. As in the case of the donor defects, within the limits of the unit cell available, the lattice distortion introduced by the acceptor defect was a symmetrical deformation about the defect center, with no reconstruction.

While the dominant effect of the donor impurities was the perturbation to the electronic structure at the conduction-band edge, principally the formation of the A_1 antibonding resonance, the introduction of Si acceptor defects leaves the conduction band virtually unaltered. The A_1A resonance of the Si_{Sb} defect is located deep into the conduction band, well away from the band edge, and as such is not expected to play a key role in determining the optical or transport characteristics. However, for the case of the acceptor impurities it is the properties of the valence-band edge states, and particularly the formation of resonances close to the valence band edge, which are of the greatest interest. Analysis of the charge densities of the valence-band states shows strong localized features at approximately 1 eV below the valence-band edge. The charge density of the principal localized resonance at this energy is shown in Fig. 10, plotted in the plane parallel to the interfaces. This is clearly seen to have T_2 symmetry, and can be identified as one of the occupied T_2B resonances predicted by the defect molecule model. The energy of this resonance relative to the valence-band edge is comparable to the energy of the A_1A resonance of the Si_{In} defect relative to the conduction-band edge. How-

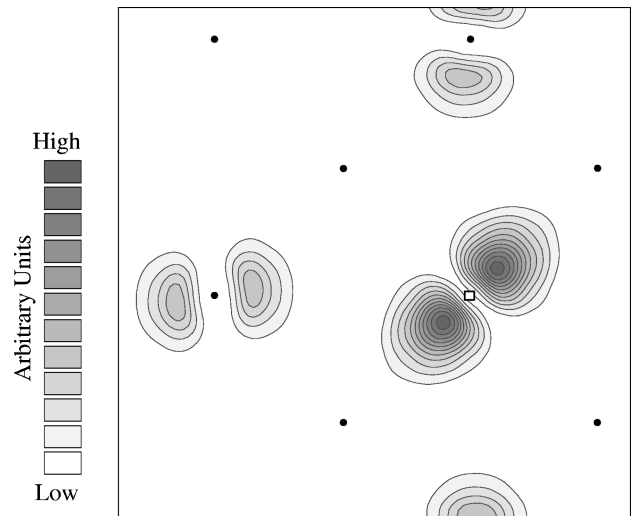


FIG. 10. The charge density (arbitrary units) associated with the T_2B resonance of the Si_{Sb} defect in the 2AlSb/2InAs superlattice, plotted in the plane parallel to the interfaces, passing through the defect atom. The projection of the positions of the Sb atoms that were located in this plane prior to relaxation are indicated by solid circles, while the open box indicates the position of the Si atom.

ever, while the form of the Si_{In} resonance in the conduction band showed a significant departure from the bulklike resonance, attributable to the defect-interface interaction, no such effect is in evidence for the Si_{Sb} T_2 bonding resonances. The form of these is essentially that which one expects in bulk, and indeed is what calculations on Si_{Sb} defects in bulk AlSb show.

VI. NEUTRAL Si-Si DEFECTS

It is interesting now to consider the possibility of a neutral defect resulting from the formation of a Si-Si pair across the InSb interface. That is, to look at the situation of a Si_{In} defect at the edge of the InAs layer bonded to a Si_{Sb} defect at the edge of the AlSb layer, where the original InSb-like bond has been replaced by a Si-Si bond. First, we must ask how likely it is that such a pair would form? To address this question we must compare the total energy associated with the defects while isolated from each other, with that of the neutral double defect. Now, the total energies that are obtained from the LDA calculations depend upon the constituent atoms of the unit cell used. A meaningful comparison of the total energy between different calculations can only be made where the same atoms are contained. As it is not practical to attempt a calculation in which the two defects are effectively isolated, since the size of unit cell required would be prohibitive, we must seek an alternative method. To make the comparison between the energies associated with the separated Si_{In} and Si_{Sb} defects and the paired defects we may add the total energies of the two separate defect calculations, and compare them with the sum of the total energies of the double defect and perfect calculations. Each combined total energy then represents the energy of a cell containing two times the unit cell of the perfect system with two defects, Si_{In} and Si_{Sb} . The difference in these energies will show whether the formation of the Si-Si defect pair is energetically favorable or not. The energy associated with the paired defect is

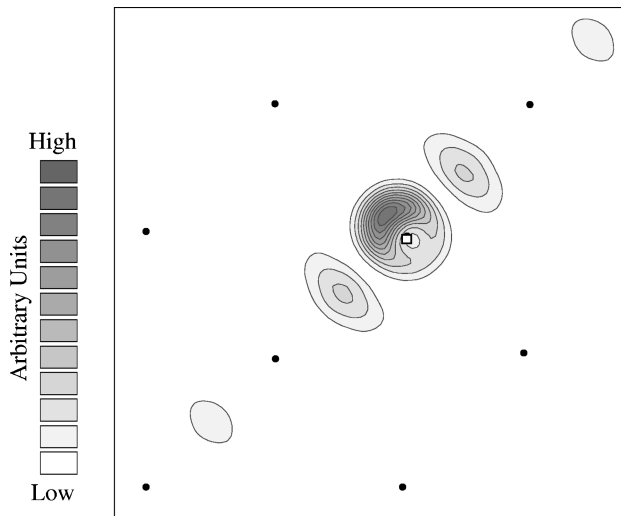


FIG. 11. The charge density (arbitrary units) associated with the A1A resonance of the $\text{Si}_{\text{In}}\text{-Si}_{\text{Sb}}$ defect pair in the 2AlSb/2InAs superlattice, plotted in the plane parallel to the interfaces, passing through the Si_{In} defect atom. The projection of the positions of the In atoms that were located in this plane prior to relaxation are indicated by solid circles, while the open box indicates the position of the Si atom.

found to be 1.1 eV lower than that of the separate defects, suggesting that the defect pair is indeed a realistic proposition.

Having established that the paired defect structure is a viable configuration, let us now consider how the effects of this defect might differ from the individual donor and acceptor impurities. An examination of the electronic structure of the conduction band shows that the A1A resonance associated with the Si_{In} donor is not strongly affected by the presence of the adjacent defect. For example, the principal A1A

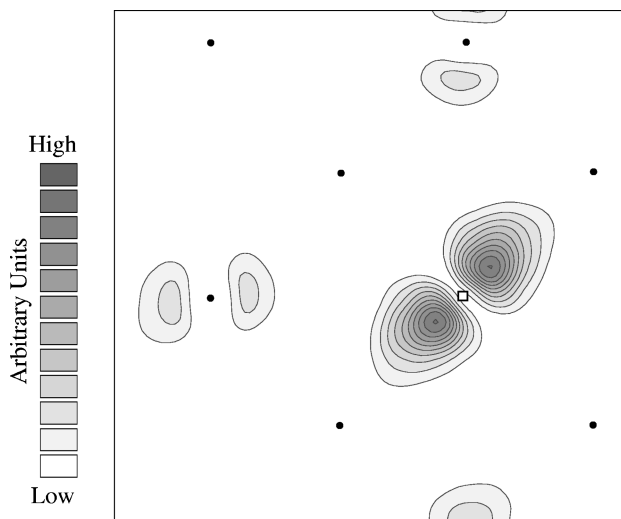


FIG. 12. The charge density (arbitrary units) associated with the T2B resonance of the $\text{Si}_{\text{In}}\text{-Si}_{\text{Sb}}$ defect pair in the 2AlSb/2InAs superlattice, plotted in the plane parallel to the interfaces, passing through the Si_{Sb} defect atom. The projection of the positions of the In atoms that were located in this plane prior to relaxation are indicated by solid circles, while the open box indicates the position of the Si atom.

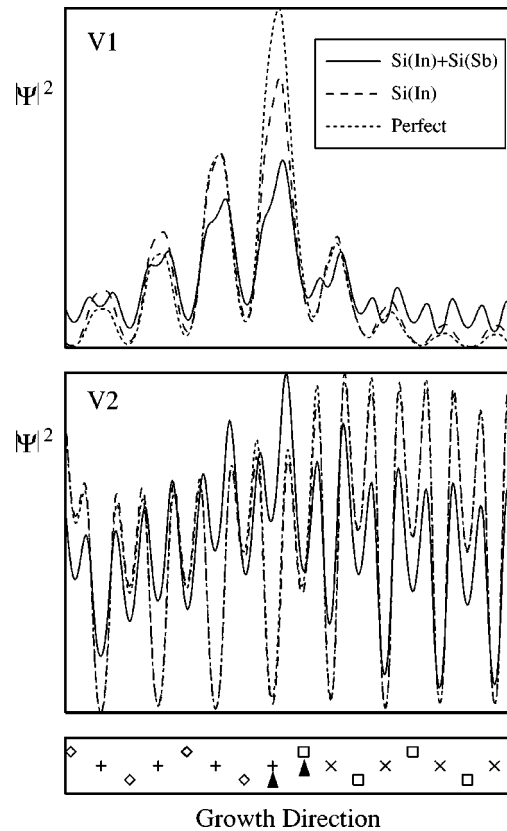


FIG. 13. The charge density (arbitrary units) of some of the zone-center states in the 2AlSb/2InAs superlattice with the $\text{Si}_{\text{In}}\text{-Si}_{\text{Sb}}$ defect pair, integrated over the plane parallel to the interface, is plotted against position along the growth axis. The charge density is shown for the two states closest to the valence-band edge. The positions of the atomic planes are indicated at the bottom where \diamond represents Al, $+$ represents Sb, \square represents In, and \times represents As. The planes in which the defects were located are indicated by the arrows.

resonance for the double defect is plotted in Fig. 11, and can be compared to the corresponding isolated donor resonance of Fig. 6, showing a similar general form. The conduction-band edge states are virtually unchanged from the single donor defect. By contrast, the valence band structure is considerably modified by the formation of the defect pair, and the consequent reduction of the crystal symmetry from C_{2v} to C_s . While the localized T2B resonance associated with the acceptor impurity is largely unaffected, and is plotted in Fig. 12, the valence-band edge states are strongly perturbed by the symmetry reduction. Figure 13 compares the valence-band edge states between the isolated Si_{Sb} defect and the $\text{Si}_{\text{In}}\text{-Si}_{\text{Sb}}$ pair. The band-edge wave functions for the isolated defect are almost unchanged from those of the perfect system. However, it can be seen clearly from Fig. 13 that in the case of the defect pair there is a considerable disturbance in the electronic states at the valence-band edge. Such a large perturbation to the valence states is likely to be reflected in modifications to the optical properties of the structure, and to the dynamics of carriers in the band.

VII. DISORDER EFFECTS

We have considered above a number of imperfect structures in which the deviation from the ideal superlattice arises

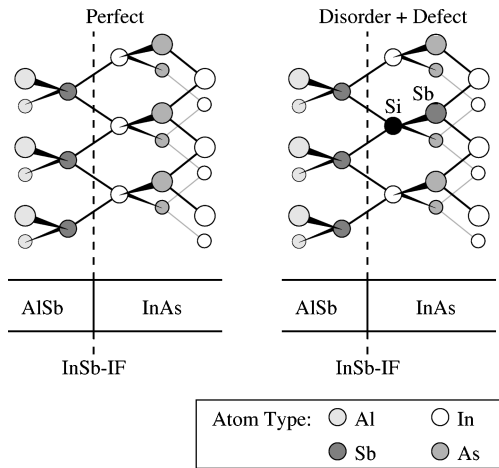


FIG. 14. A schematic diagram showing the disordered atomic structure studied. The perfect system is shown on the right, while the left shows the position of the Si_{In} donor defect and the Sb_{As} atom representing disorder in the structure.

through the inclusion of a foreign impurity atom (or atoms). Of course, it is also likely that there will be some disorder in the arrangement of the superlattice constituents, both due to the growth of the interface itself and in the vicinity of an impurity. While the case of simple disorder at the interfaces of InAs/AlSb, involving no foreign impurity species, was found to have only a relatively small effect,³¹ it is interesting to ask how disorder might affect the localized features that result from the presence of impurity defects. That is, to consider how the defect-interface interaction is influenced by the presence of disorder. This will provide a link between the quality of superlattice growth and the localization features that have been identified. For the present purposes it is not appropriate to attempt a comprehensive study of the very many disorder/defect configurations that might occur. Rather, we shall restrict ourselves to consideration of a single representative case that should indicate the general effects that can be expected from such disorder. We shall concentrate on the substitutional Si_{In} donor defect studied in detail in Sec. III, and examine how this system is affected by the inclusion of an adjacent Sb_{As} disorder substitution. The geometry of the disorder-defect configuration that we consider is illustrated schematically in Fig. 14. This particular configuration has been chosen to represent both a relatively likely disordered structure and one that might be expected to give rise to interesting behavior.

To identify the disorder-related effects from this calculation we must compare directly with the case of the lone Si_{In} defect. The charge density of the $A1A$ resonance of the disordered structure is plotted in the plane of the Si defect atom in Fig. 15. Comparison with the perfect Si_{In} defect structure shows a rather significant modification to the localized feature by just this single Sb_{As} atom. While the nature of the localization, and the general interface-induced perturbation to the bulklike resonance, remain clearly visible in the resonance, it is apparent that the detailed form and symmetry of the localized feature are affected by the presence of the disorder. Thus, importantly, we note that although the interfacial disorder is not itself capable of inducing a localized state, it is sufficient to significantly alter the localized reso-

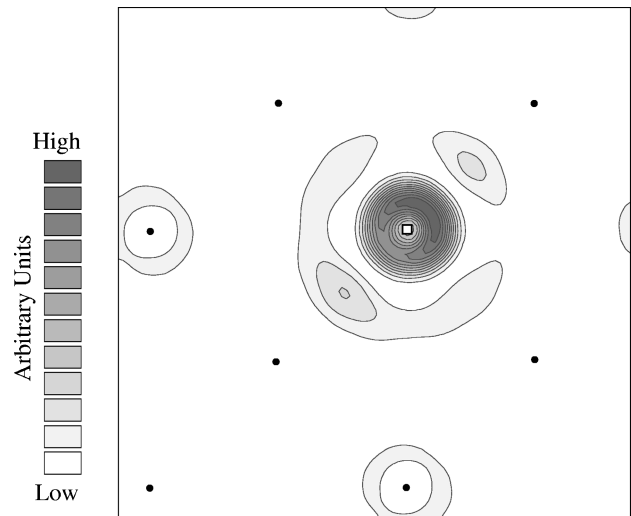


FIG. 15. The charge density (arbitrary units) associated with the $A1A$ resonance of the Si_{In} defect in the $2\text{AlSb}/2\text{InAs}$ superlattice with Sb_{As} disorder, plotted in the plane parallel to the interfaces, passing through the Si_{In} defect atom. The projection of the positions of the In atoms that were located in this plane prior to relaxation are indicated by solid circles, while the open box indicates the position of the Si atom.

nance associated with the Si defect.

Returning to the issue of the optical characteristics of the structures, it is now possible to envisage a mechanism by which the selection rules associated with the idealized structures might break down. The presence of a substitutional defect atom in the vicinity of the superlattice interface results in highly localized interface-related features. The effect of interface disorder, minimized in impurity-free quantum wells through the localization of the conventional ground state near the center of the quantum wells, is enhanced by the defect-induced interface resonance, which results in a large ‘‘sampling’’ of the disorder. The presence of the donor impurity in the interface region thus provides the means by which a breakdown in order at the interface, to a degree that would be expected with even the highest quality growth foreseeable, can play a significant role in the determination of the optical response.

VIII. CONCLUSION

In conclusion, we have applied *ab initio* pseudopotential calculations to the study of a series of imperfect AlSb/InAs superlattices. An interface-induced localization in the presence of substitutional Si_{In} donor defects has been identified, analogous to the localization predicted at donors in SiGe structures. The form of the localization has been shown to be specific to the chemical nature of the defect atom. Further, the form of the resonance is sensitive to interfacial disorder, and provides a possible link between the quality of the interfaces and the optical spectra of the microstructures. The resonances associated with Si_{Sb} acceptor defects have also been studied, though these are not found to be sensitive to the presence of the interfaces. Finally, a Si-Si defect pair located across the InSb-like interfaces has been shown to be energetically favorable, and to give rise to interface-induced localized resonances close to the conduction-band edge, simi-

lar to the single Si donor defect. Such a defect pair also introduces a significant perturbation to the electronic structure at the valence-band edge.

The localized interface features that have been described cannot be obtained using conventional semiclassical models of the interface potential, but rather require a full microscopic model such as the *ab initio* approach used in this study. Only by including the microscopic variations in potential that occur in the region of the interface bonds themselves, can such effects be accounted for. The results presented in this paper demonstrate that these microscopic interfacial properties—the “intraface” parameters—provide a key to an understanding of heterostructure behavior, that

goes beyond that which may be obtained from conventional heterostructure theory.

ACKNOWLEDGMENTS

I would like to thank the U.K. Engineering and Physical Science Research Council, D.E.R.A. (Malvern), and the Office of Naval Research (U.S.A.) for financial support. I also thank P. R. Briddon and M. Jaros at the University of Newcastle upon Tyne for many helpful discussions, and in particular P. R. Briddon for providing invaluable computer codes.

-
- ¹R. J. Turton and M. Jaros, *Appl. Phys. Lett.* **69**, 2891 (1996).
²M. J. Shaw, P. R. Briddon, and M. Jaros, *Phys. Rev. B* **54**, 16 781 (1996).
³M. J. Shaw, P. R. Briddon, and M. Jaros, *Phys. Rev. B* **52**, 16 341 (1995).
⁴A. Y. Lew, S. L. Zuo, E. T. Yu, and R. H. Miles, *Appl. Phys. Lett.* **70**, 75 (1997).
⁵R. M. Feenstra, D. A. Collins, D. Z.-Y. Ting, M. W. Wang, and T. C. McGill, *Phys. Rev. Lett.* **72**, 2749 (1994).
⁶R. G. Dandrea and C. B. Duke, *Appl. Phys. Lett.* **63**, 1795 (1993).
⁷I. Sela, C. R. Bolognesi, L. A. Samoska, and H. Kroemer, *Appl. Phys. Lett.* **60**, 3283 (1992).
⁸M. Gail, G. Abstreiter, J. Olajos, J. Engvall, H. Grimmeiss, H. Kibbel, and H. Presting, *Appl. Phys. Lett.* **66**, 2978 (1995).
⁹J. Engvall, J. Olajos, H. Grimmeiss, H. Kibbel, and H. Presting, *Phys. Rev. B* **51**, 2001 (1995).
¹⁰M. Gail, W. Jung, J. Brunner, P. Schittenhelm, J. F. Nützel, and G. Abstreiter, *Solid State Phenom.* **47-48**, 473 (1996).
¹¹M. Jaros, *Semicond. Semimet.* **32**, 175 (1990), and references within.
¹²R. J. Turton and M. Jaros, *Semicond. Sci. Technol.* **8**, 2003 (1993).
¹³D. E. Jesson, S. J. Pennycook, and J.-M. Baribeau, *Phys. Rev. Lett.* **66**, 750 (1991).
¹⁴S. Froyen, D. M. Wood, and A. Zunger, *Phys. Rev. B* **37**, 6893 (1988).
¹⁵S. Satpathy, R. M. Martin, and C. G. Van de Walle, *Phys. Rev. B* **38**, 13 237 (1988).
¹⁶U. Schmid, N. E. Christensen, M. Alouani, and M. Cardona, *Phys. Rev. B* **43**, 14 597 (1991).
¹⁷D. L. Smith and C. Mailliot, *J. Appl. Phys.* **62**, 2545 (1987).
¹⁸R. H. Miles, D. H. Chow, J. N. Schulman, and T. C. McGill, *Appl. Phys. Lett.* **57**, 801 (1990).
¹⁹J. L. Johnson, L. A. Samoska, A. C. Gossard, J. L. Merz, M. D. Jack, G. R. Chapman, B. A. Baumgratz, K. Kosai, and S. M. Johnson, *J. Appl. Phys.* **80**, 1116 (1996).
²⁰H. Xie, W. I. Wang, J. R. Meyer, C. A. Hoffman, and F. J. Bartoli, *J. Appl. Phys.* **74**, 2810 (1993).
²¹M. J. Shaw and M. Jaros, *Phys. Rev. B* **50**, 7768 (1994).
²²G. Tuttle, H. Kroemer, and J. H. English, *J. Appl. Phys.* **65**, 5239 (1989).
²³J. Wagner, J. Schmitz, F. Fuchs, J. D. Ralston, P. Koidl, and D. Richards, *Phys. Rev. B* **51**, 9786 (1995).
²⁴B. Brar, J. Ibbetson, H. Kroemer, and J. H. English, *Appl. Phys. Lett.* **64**, 3392 (1994).
²⁵J. Spitzer, A. Höpner, M. Kuball, M. Cardona, B. Jenichen, H. Neuroth, B. Brar, and H. Kroemer, *J. Appl. Phys.* **77**, 811 (1995).
²⁶G. Tuttle, H. Kroemer, and J. H. English, *J. Appl. Phys.* **67**, 3032 (1990).
²⁷H. Kroemer, C. Nguyen, and B. Brar, *J. Vac. Sci. Technol. B* **10**, 1769 (1992).
²⁸S. Ideshita, A. Furukawa, Y. Mochizuki, and M. Mizuta, *Appl. Phys. Lett.* **60**, 2549 (1992).
²⁹D. J. Chadi, *Phys. Rev. B* **47**, 13 478 (1993).
³⁰J. Shen, H. Goronkin, J. D. Dow, and S. Y. Ren, *J. Appl. Phys.* **77**, 1576 (1995).
³¹M. J. Shaw, P. R. Briddon, and M. Jaros, *Solid State Phenom.* **47-48**, 491 (1996).
³²M. J. Shaw, G. Gopir, P. R. Briddon, and M. Jaros, *J. Vac. Sci. Technol. B* (to be published).
³³For example, R. M. Dreizler and E. K. U. Gross, *Density Functional Theory: An Approach to the Quantum Many-Body Problem* (Springer-Verlag, Berlin, 1990), and references within.
³⁴G. B. Bachelet, D. R. Hamann, and M. Schlüter, *Phys. Rev. B* **26**, 4199 (1982).
³⁵R. Jones, *J. Phys. C* **21**, 5735 (1988).
³⁶P. R. Briddon, Ph.D. thesis, University of Exeter, U. K.
³⁷M. Jaros, *Deep Levels in Semiconductors* (Adam Hilger, Bristol, U.K., 1982).
³⁸M. J. Shaw and M. Jaros, *Semicond. Semimet.* (to be published).